Probing Modified Gravitational Wave Dispersion with Bursts from Eccentric Binaries

Ava Bailey,[1,*] Nicholas Loutrel,[2,3,†] and Davide Gerosa[2,3,4]

[1] *Department of Physics, Duke University, 120 Science Drive, Durham, NC 27708, USA*
[2] *Dipartimento di Fisica "G. Occhialini", Universitá degli Studi di Milano-Bicocca, Piazza della Scienza 3, 20126 Milano, Italy*
[3] *INFN, Sezione di Milano-Bicocca, Piazza della Scienza 3, 20126 Milano, Italy*
[4] *School of Physics and Astronomy & Institute for Gravitational Wave Astronomy, University of Birmingham, Birmingham, B15 2TT, UK*

(Dated: August 2, 2024)

I. INTRODUCTION

With the increasing number of modified general relativity (GR) theories and new models of gravitational physics, we search to bridge the theoretical gaps in the current model of our universe. To fully understand where and when certain theories hold, we must holistically investigate the implications of such modifications. Within the scope of gravitational physics, the effect of non-GR phenomena have been studied for low and moderate eccentricity binaries, but never robustly for the high-eccentricity regime. In this study we aim to thoroughly derive gravitational wave (GW) waveforms in the time and frequency domain for high-eccentricity binaries with the goal of evaluating the impact of GR modifications on these waveforms to better constrain GW parameters under both GR and non-GR phenomena.

The purpose of studying high-eccentricity binaries is highlighted in [1] where the comparison of radiated energy in circular and eccentric binaries is evaluated as a function of luminosity. Eccentric binaries produce a greater proportion of their radiated GW power in the high-luminosity regime as compared to circular binaries. This is useful because, along with having more GW radiation, certain system parameters scale with the luminosity of the system. Having larger parameter values allows for better constraining compared to smaller parameter estimations where both estimates may have the same error prediction.

One particular area of interest within parameter constraints is the assessment of GR and modified GR theories. Under non-GR phenomena, the parameters used to construct GW waveforms become modified depending upon which non-GR phenomenon is being injected into the waveform. By studying eccentric binaries under both GR and modified GR scenarios, we can recover better constraints on varying theorized parameters to test the validity of different universal theories by assessing how well these recovered parameters match known system parameters.

The report follows the general format of first providing a primer on modifications to GR and how to derive parameter estimations for various dispersive effects to be used in dispersive time offsets in Sec. II. Then we modify existing time-domain waveforms to implement dispersive effects in high-eccentricity waveforms in Sec. III. Then we turn to the frequency domain and implement the effective-fly-by framework to derive dispersive, high-eccentricity waveforms in Sec. IV. In Sec. V we take these waveforms and develop a timing model over which the waveforms evolve for multiple sequential orbits to accurately model the binary inspiral. We go on to discuss continuations of this investigation in Sec. VI, and we recommend next steps to thoroughly evaluate our newly derived waveforms and timing model for the sake of validating and estimating parameters from non-GR phenomena. Lastly, we present a detailed derivation of the waveforms from the effective-fly-by framework in Sec. A as used in Sec. IV.

II. MODIFIED GRAVITATIONAL WAVE DISPERSION: A PRIMER

Under GR, GWs propagate at the speed of light with the velocity of the wavefront being constant and independent of any influence from the originating system. In some scenarios in which GR is modified, the speed of propagation becomes frequency dependent. This frequency dependence is a result of dispersion or dispersive effects which cause the waveform to oscillate and disperse as waves of different frequencies travel with different speeds and arrive at the detector at varying times.

A host of different non-GR phenomena can modify the propagation of GWs, but only a subset of these result in dispersion. Dispersion effects may be captured in the GWs through the parameterized dispersion relation [2–4]

$$\omega^2 = k^2 + \alpha L_P^{2a-4} k^a, \tag{1}$$

where (ω, k) are the angular frequency and wave number of the graviton, and (α, a) are non-GR parameters that capture the strength and type of dispersion effect, respectively. The above parameterized dispersion relation causes GWs at different frequencies to propagate at different velocities, which can be seen from the group velocity of the gravitons, specifically

$$v_g = \frac{d\omega}{dk} = 1 + \frac{(a-1)}{2}\alpha L_P^{2a-4}\omega^{a-2}\,. \tag{2}$$

* ava.bailey@duke.edu
† nicholas.loutrel@unimib.it

Due to the modification of the above group velocity, gravitons emitted at the same instant, but at different frequencies, will arrive at a GW detector at different times. A thorough calculation of this effect, including the influence of cosmological redshift, can be found in [4]. For simplicity, we neglect the effect of cosmological backgrounds, and thus, for two gravitons of frequency (f, f') and emitted at times (t_e, t'_e), the observed times of arrival are related by

$$\Delta t_o = \Delta t_e + \frac{D_L}{2\lambda_\alpha^{2-a}}\left(\frac{1}{f^{2-a}} - \frac{1}{f'^{2-a}}\right), \tag{3}$$

where D_L is the (luminosity) distance to the source, $\Delta t_{o,e} = t_{o,e} - t'_{o,e}$, and

$$\lambda_\alpha = 2\pi L_P^2 \alpha^{1/(a-2)}, \tag{4}$$

which is the "wavelength" associated with α.

The parameters (α, a) map to specific non-GR scenarios. Many of these arise due to the introduction of a minimal length scale and the breaking of Lorentz invariance, since these concepts are usually connected. A few examples include:

- *Massive gravitons* [5–8]: The simplest, and largely phenomenological, deviation is for gravitons to possess a mass m_g. In this case, the dispersion relation obtains a momentum/wave number independent term. Thus $\alpha = m_g^2$ and $a = 0$, and hence $\lambda_g = 2\pi L_P^2/m_g$ is the Compton wavelength of the graviton.

- *Extra dimensions* [9]: A postulated dispersion relation obtained by comparing to a generalized uncertainty principle in a universe with extra dimensions reveals $\alpha = -\alpha_{\rm edt}/L_P^4$ and $a = 4$, where $\alpha_{\rm edt}$ is related to the length scale of the extra dimensions. This is typically considered to be the Planck length L_p and $\alpha_{\rm edt} \sim L_P^2$, the value of which, in this case, depends on the number of spacetime dimensions.

- *Doubly special relativity* [10–12]: A modification of special relativity through nonlinear modification of the Lorentz group by introducing an invariant length/momentum scale, in addition to the invariant speed of light. The length scale is taken to be the Planck length, and in the limit of the wavelegth of the wave being much larger than this scale, $\alpha = \eta_{\rm drst}/L_P^2$ and $a = 3$, where $\eta_{\rm drst}$ is commonly related to the Planck length, i.e. $\eta_{\rm drst} \sim L_P$.

- *Hořava-Lifschitz gravity* [13–16]: A proposed quantum theory of gravity that introduced a preferred time foliation, such that Lorentz invariance only arises at large distances compared to the Planck length. In this theory, GWs obey a dispersion relation with $\alpha = \kappa_{hl}^4 \mu_{hl}^2/16$ and $a = 4$, where $(\kappa_{\rm hl}, \mu_{\rm hl})$ are coupling constants of the theory related to the bare gravitational constant and balance conditions of the theory, respectively.

- *Multifractional spacetime theory* [17–20]: Another proposed quantum theory of gravity that allows the effective dimension of spacetime to vary at different scales by replacing the D-dimensional measure of the action $d^D x$ with a Lebesgue-Stieltjes measure $d\rho(x)$. For this theory, the GW dispersion relation takes different forms depending on the preferred foliation of the spacetime. For timelike factal foliations, $\alpha = 2\omega_\star^{2-a}/(3-a)$, while for spacelike fractal foliations $\alpha = -2 \times 3^{1-a/2}\omega_\star^{2-a}/(3-a)$, with $\omega_\star$ a characteristic frequency (energy) scale. For both scenarios, a need not be an integer values, but $a = 2 - 3$ and typically one choses $a = 2.5$.

- *Gravitational standard model extension (SME)* [21]: An effective field theory that combines the standard model of particle physics with GR, and includes Lorentz symmetry breaking. The exact form of the modified dispersion relation varies depending on the dimension of the Lorentz breaking operators introduced into the action. For even $d \geq 4$, $\alpha = -2k^{(d)}_{(I)}$, while for odd $d \geq 5$, $\alpha = \pm k^{(d)}_{(V)}$, and $a = d - 2$. The constant coefficients $k^{(d)}_{(I,V)}$ control the Lorentz violating operators in the action.

The above list is far from exhaustive, but provides a general sense of the physics that the modified dispersion relation in Eq. (1) captures. In the next section, we will visually show the imprint of a few of these cases on the propagation of eccentric bursts.

III. ECCENTRIC BINARIES AND TIME-DOMAIN GRAVITATIONAL WAVES

The first formulation of the GW waveform for eccentric binaries was derived by Wahlquist [22] and later reformed with newer notation by Martel and Poisson [23]. We follow Martel and Poisson and define the GW polarizations as:

$$\begin{aligned} h_+ = -\frac{m\eta}{pD_L}\Big\{\Big[2\cos(2\phi - 2\beta) + \frac{5}{2}e\cos(\phi - 2\beta) + \\ \frac{1}{2}e\cos(3\phi - 2\beta) + e^2\cos 2\beta\Big](1 + \cos^2\iota) + \\ [e\cos\phi + e^2]\sin^2\iota\Big\}, \end{aligned} \tag{5}$$

and

$$\begin{aligned} h_\times = -\frac{m\eta}{pD_L}[4\sin(2\phi - 2\beta) + 5e\sin(\phi - 2\beta) + \\ e\sin(3\phi - 2\beta) - 2e^2\sin 2\beta]\cos\iota, \end{aligned} \tag{6}$$

where β and ι are the angles that define the polarization axes, η is the symmetric mass ratio, m is the total mass of the system, p is the semilatus rectum which is related

to eccentricity and semi-major axis by $p = a(1-e^2)$, and D_L is the luminosity distance.

The time-domain signal of the waveforms can be decomposed into harmonics of the mean orbital frequency which shows the time dependence of the field component equations [24, 25]:

$$h_{+,\times}(t) = -h_0 \sum_{k=1}^{\infty} \Big[S^{(k)}_{+,\times} \sin(k\ell) + C^{(k)}_{+,\times} \cos(k\ell) \Big], \quad (7)$$

where we introduce the notation used by Moore et al. [25] such that the coefficients $S^{(k)}_{+,\times}$ and $C^{(k)}_{+,\times}$ are functions of eccentricity and the polarization angles and h_0 is dependent upon the individual masses of the binary constituents, semi-major axis, eccentricity, and luminosity distance. These coefficients are explicitly defined as:

$$S^{(k)}_{+} = \frac{4}{e^2}[1+\cos^2\iota]\sin 2\beta\sqrt{1-e^2}\Big\{eJ_{k-1}(ke) - [1+k(1-e^2)]J_k(ke)\Big\}, \quad (8)$$

$$C^{(k)}_{+} = \frac{2}{e^2}\Big\{\Big[\cos 2\beta(1+\cos^2\iota)e(1-e^2)k\big(J_{k+1}(ke) - J_{k-1}(ke)\big)\Big] - \Big[\cos 2\beta(1+\cos^2\iota)(e^2-2) + e^2\sin^2\iota\Big]J_k(ke)\Big\}, \quad (9)\text{–}(10)$$

$$S^{(k)}_{\times} = \frac{8}{e^2}\cos 2\beta\cos\iota\sqrt{1-e^2}\Big\{eJ_{k-1}(ke) - [1+(1-e^2)k]J_k(ke)\Big\}, \quad (11)$$

$$C^{(k)}_{\times} = \frac{4}{e^2}\sin 2\beta\cos\iota\Big\{2e(1-e^2)kJ_{k-1}(ke) - 2\Big[1+(1+e^2)k-\frac{e^2}{2}\Big]J_k(ke)\Big\}, \quad (12)$$

$$h_0 = \frac{2m_1m_2}{a(1-e^2)}\frac{2}{D_L}. \quad (13)$$

Eq. (7) is also dependent upon the mean anomaly ℓ which is given as $\ell = 2\pi(t-t_p)F_{\rm orb}$, with $F_{\rm orb}$ being the orbital frequency, and t_p the time of pericenter passage.

These waveforms describe a continuous radiative signal that is non-dispersive. Under modifications to GR, the waveforms become dispersive requiring the study and consideration of time shifts between the time at which GWs are emitted and when they are observed. At leading PN order, quasi-circular binaries only emit GWs at twice the orbital frequency, which can be seen by taking the limit $e \to 0$ of Eqs. (5)-(6). As a result, dispersion effects modify the the observed frequency evolution of the binary (see [4] for details). However, comparison to the eccentric case in Eq. (7) reveals that eccentric binaries emit GWs in many orbital harmonics simultaneously. Since each harmonic possesses a different frequency, they will arrive at the detector at different times, resulting in an observed modulation of the waveform. Here, we are primarily interested in the high eccentricity limit, where the waveforms resemble discrete bursts instead of continuous waves. While the discussion will primarily focus on this case, the formalism we develop here is general enough to apply to low and moderately eccentric systems as well.

In our initial discussion of mean anomaly ℓ as is included in Eq. (7), we highlighted that ℓ is a function of time t where, under GR, time is measured absolutely without distinction between emitted and observed times. Under dispersion effects and modifications to GR, the time t which characterizes the mean anomaly maps to emitted time t_e, considering this is the absolute time at which the GW is radiated as measured in respect to the system and the system's time of pericenter passage. This would mean that under dispersion, the mean anomaly should be expressed as $\ell_e = 2\pi F_{\rm orb}(t_e - t_p^{(e)}) = 2\pi F_{\rm orb}\Delta t_e$, where $t_p^{(e)}$ is the "emitted" time of pericenter passage, and we relabel ℓ with the 'e' subscript to indicate its dependence on the emitted time. Each harmonic in Eq. (7) will propagate at a different velocity, and will thus be observed at time t_o. We further define $\ell_o = 2\pi F_{\rm orb}(t_o - t_p^{(o)}) = 2\pi F_{\rm orb}\Delta t_o$, with $t_p^{(o)}$ the "observed" time of pericenter passage. For the k-th harmonic of the waveform, the quantities ℓ_o and ℓ_e are then related to each other by Eq. (3) taking $f = kF_{\rm orb}$,

$$\ell_o = \ell_e + \frac{\pi D_L}{\lambda_\alpha^{2-a}F_{\rm orb}^{1-a}}\left(\frac{1}{k^{2-a}} - \frac{1}{k_{\rm max}^{2-a}}\right), \quad (14)$$

where we have also chosen $f' = k_{\rm max}F_{\rm orb}$, with [26]

$$k_{\rm max} = \frac{2(1+e)^{1.1954}}{(1-e^2)^{3/2}}, \quad (15)$$

which corresponds to the harmonic with maximum power.

We have made two choices to arrive at Eq. (14), namely that the constant time shifts physically associated with pericenter passage $[t_p^{(e)}, t_p^{(o)}]$ are different for $[\ell_e, \ell_o]$, and that the reference frequency f' is chosen to be fixed at $k_{\rm max}F_{\rm orb}$. Both of these stem from the burst formalism originally developed for power stacking searches in [1]. There, eccentric bursts were treated as regions of excess power in a time-frequency spectrogram, each of which possessing a central coordinate (t_i, f_i). Since the modelling therein was performed in the context of GR (i.e. no dispersion), the time centroid is trivially the time of pericenter passage of the orbit from which the burst originates, while the frequency centroid is related to the peak of the waveform power spectrum or amplitude. The former can be mapped to the pericenter passage time of the previous orbit by incorporating radiation reaction effects into a timing model, which we will discuss in more detail in Sec. V. The latter was first considered by Turner [27], who showed that the peak of the power spectrum for nearly parabolic orbits is related to the characteristic timescale of pericenter passage, although a more thorough computation was carried out in [26], leading to Eq. (15). Making these choices will allow us to address how the time-frequency centroid of each burst is modified due to dispersion effects in Sec. V.

At this point, we may implement the dispersion effects into the time-domain waveform. We are able to express Eq. (7) with an exponential term harmonic coefficients dependent upon $S^{(k)}_{+,\times}$ and $C^{(k)}_{+,\times}$ through manipulating Euler's formula. This gives a new, equivalent expression for the polarizations,

$$h_{+,\times}(t_e) = -h_0 \sum_{k=1}^{\infty} \left[H^{(k)}_{+,\times} e^{ik\ell_e} + \left(H^{(k)}_{+,\times} \right)^{\dagger} e^{-ik\ell_e} \right], \quad (16)$$

where $H^{(k)}_{+,\times} = (C^{(k)}_{+,\times} - iS^{(k)}_{+,\times})/2$, and $\dagger$ indicates the complex conjugate of the specified terms. Now that the time-dependent term ℓ_e has been isolated into an exponential term, we use Eq. (14) to separate the exponential into a product of two terms one of which depends solely on ℓ_o and another which is time-independent, specifically

$$e^{ik\ell_e} = B_k(\bar{\alpha}) e^{ik\ell_o}\,, \quad (17)$$

where

$$B_k(\bar{\alpha}) = \exp\left\{ \frac{i}{2}\bar{\alpha} k^{a/2} \left[\left(\frac{k}{k_{\rm max}} \right)^{1-\frac{a}{2}} - \left(\frac{k}{k_{\rm max}} \right)^{\frac{a}{2}-1} \right] \right\}, \quad (18)$$

with the dimensionless coupling parameter

$$\bar{\alpha} = \frac{2\pi D_L k_{\rm max}^{(a/2)-1}}{\lambda_\alpha^{2-a} F_{\rm orb}^{1-a}}\,. \quad (19)$$

Thus, the final expression of the dispersion modulated waveform is

$$\begin{aligned} h_{+,\times}(t_o) = &- h_0 \sum_{k=1}^{\infty} \Big\{ H^{(k)}_{+,\times} B_k(\bar{\alpha}) e^{ik\ell_o} \\ &+ \left(H^{(k)}_{+,\times} \right)^{\dagger} B^{\dagger}_k(\bar{\alpha}) e^{-ik\ell_o} \Big\}, \end{aligned} \quad (20)$$

where recall that ℓ_o is related to the time at which the GWs are observed.

In Fig. 1 we show an illustrative plot of the dispersion modulated time-domain waveform plotted against the GR waveform for three different GR-modified scenarios: massive gravitons, extra dimensions, and doubly special relativity. We reference Eq. (19) in the plot titles to give clear values of $\bar{\alpha}$ which correspond to the changing values of luminosity distance which we set at 10 Mpc, 100 Mpc, and 1000 Mpc for each different non-GR scenario. Fig. 1 serves as a useful visualization for the GW burst distortion in the time domain as a result of dispersion implementation where the severity and behavior of the distortion depend upon various parameters that we use to characterize $\bar{\alpha}$ including λ_α and a which, again, define the strength and type of dispersion effect respectively.

IV. DISPERSION EFFECTS IN FREQUENCY-DOMAIN ECCENTRIC BURST WAVEFORMS

The discussion of the previous section functions for both illustrative purposes, as well as to devise a general formalism of how to adjust for non-GR dispersion effects in eccentric PN waveforms. However, these are not the most useful for performing studies of projected constraints on non-GR effects, and we must move to the frequency domain to do so. This can be performed numerically, but to limit numerical error in our final results, we focus on implementing the dispersion effects into analytic frequency-domain eccentric waveforms. To do this, we break from the generality of the previous section, and restrict our attention to GW bursts from highly eccentric sources, which may be described by the effective fly-by (EFB) framework [28]. We will use a slightly modified EFB-F waveform which is derived in Appendix A herein, which we will refer to as EFB-D waveforms.

The EFB-D waveforms in the absence of dispersion are obtained by double application of the SPA, first to transform from the time-domain waveform in Eq. (7), and second to perform the resummation of the sum over k in the frequency domain. To implement dispersion effects into this, we must Fourier transform Eq. (20) which has the dispersion effect implemented in the time-domain polarizations, and determine whether either SPA is corrected by the introduction of such effects. First, the evolution of the binary under leading PN order radiation reaction is given by Eqs. (A1)-(A3) where t is promoted to t_e, and subsequently, ℓ is promoted to ℓ_e. One can rigorously show that these expressions do not change when mapping to (t_o, ℓ_o), since $\partial t_o/\partial t_e = 1$ from Eq. (3). However, there is a simpler, and more physical, reason for this, specifically, Eqs. (A1)-(A3) are related to the generation of the waves from the binary, and thus, dispersion should not alter them.

The second application of the SPA, to perform the resummation over k, can be modified due to $B_k(\bar{\alpha})$ in Eq. (18). If the dispersion effects are large, the phase of $B_k(\bar{\alpha})$ can dominate over the phase $\Psi_\star(k, f)$ in Eq. (A7). However, we are interested in parameterized tests of GR, for which the region of parameter space of interest is $\bar{\alpha} \ll 1$, since this is relevant dimensionless quantity for dispersion effects in eccentric binaries. Under this assumption, the dispersion effects should be small, and thus a slowly varying function compared to the orbital contribution to the phase from ℓ_o. We can then use the generating function of Bessel functions of the first kind,

$$e^{(z/2)(x-x^{-1})} = \sum_{m=-\infty}^{\infty} x^m J_m(z)\,, \quad (21)$$

to recast the phase modulation of $B_k(\bar{\alpha})$ into an amplitude modulation, specifically

$$B_k(\bar{\alpha}) = \sum_{m=-m_{\rm max}}^{m_{\rm max}} \left(\frac{k}{k_{\rm max}} \right)^{m(1-a/2)} J_m\left(i\bar{\alpha} k^{a/2} \right), \quad (22)$$

where we have introduced $m_{\rm max}$ to allow for the summation over m to be truncated at a finite value. The observed waveform is still given by Eq. (20), but with $B_k(\bar{\alpha})$ now given by Eq. (22).

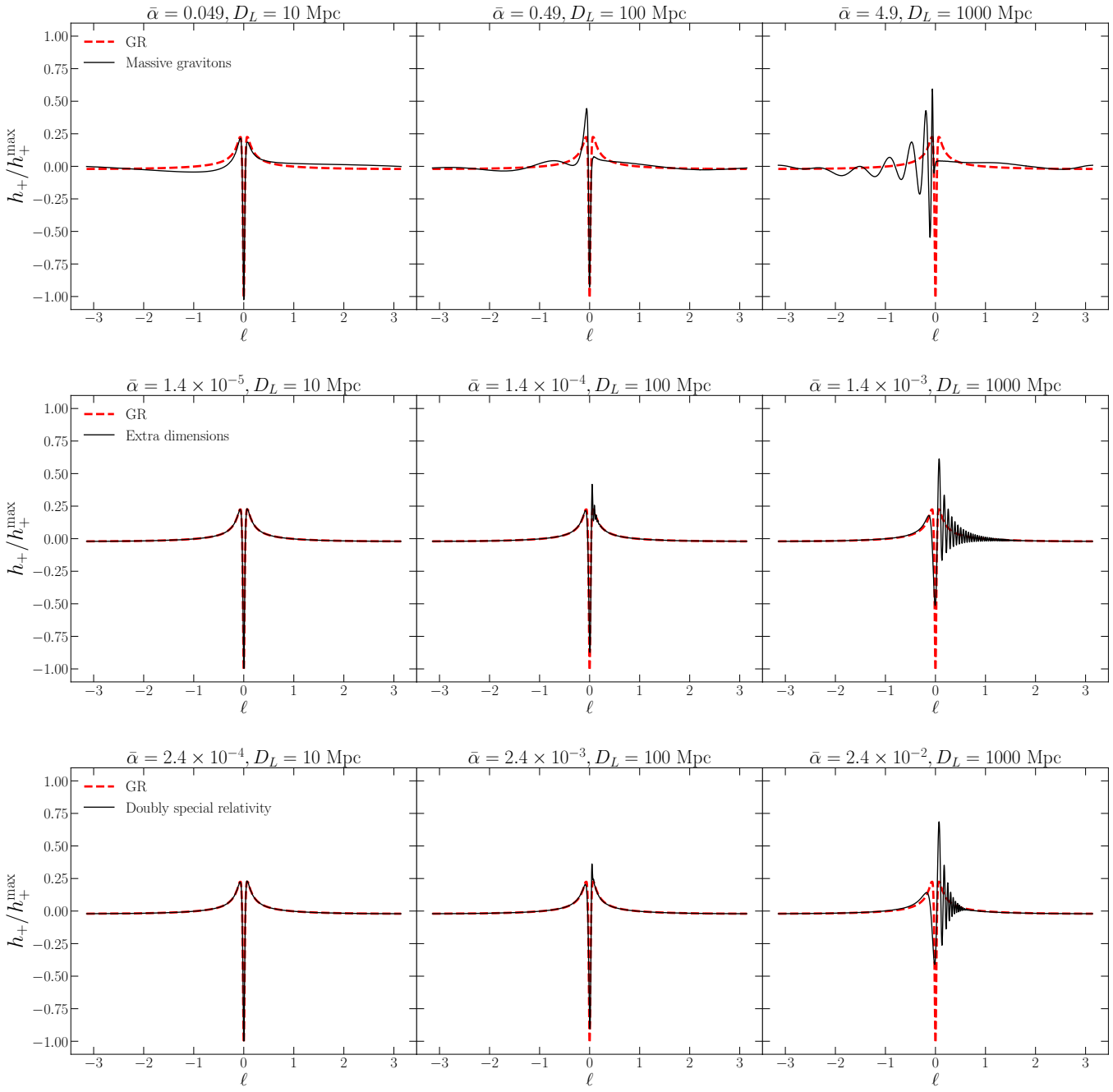

FIG. 1. Comparisons of time-domain, normalized plus-polarization waveforms under GR and three different dispersive cases: massive gravitons (uppermost panel), extra dimensions (middle panel), and doubly special relativity (bottommost panel). The dashed, red line represents the GR waveform while the black solid lines show the different dispersive waveforms for different values of $\bar{\alpha}$ which assume different values as D_L — which we set at 10 Mpc, 100 Mpc, and 1000 Mpc — increases as denoted by the plot titles. The waveforms are computed using the following parameters: $e = 0.9$, $m = 20M_\odot$, $p = 20m$, $\eta = 0.25$

Mathematically, $m_{\max} \to \infty$ in order for Eq. (22) to be an exact analytical representation of Eq. (18). However, considering the numerical impossibility of evaluating such a sum over infinite bounds, we must find adequate limits on the summation to recover an accurate value while also maintaining computational viability. From the standpoint of tests of GR, $\bar{\alpha} \ll 1$, and since $J_m(i\bar{\alpha}k^{a/2}) \sim \bar{\alpha}^m$ in this limit, one should choose $m_{max} = 1$ when preforming tests of the null hypothesis. For more general cases where $\bar{\alpha}$ can take any arbitrary value, $m_{\max} > 1$ and must be chosen such that Eq. (22) is a sufficiently accurate approximation of Eq. (18).

The frequency-domain waveform can now be obtained

by computing

$$\tilde{h}^{(o)}_{+,\times}(f) = \int dt_o h_{+,\times}(t_o) e^{2\pi i f t_o}\,, \tag{23}$$

where $h_{+,\times}(t_o)$ is given by Eq. (20) with $B_k(\bar{\alpha})$ given in Eq. (22). The time integral over t_o and resummation over k can now be computed using the exaxt same methods as detailed in Appendix A, thus we may write the final waveform directly,

$$\tilde{h}^{(o)}_{+,\times}(f) = \tilde{h}_0 \mathcal{A}_{+,\times}(f) e^{2\pi i f t^{(o)}_p}\,, \tag{24}$$

where

$$\tilde{h}_0 = -\frac{2\pi}{D_L}\left(\frac{\mathcal{M}}{n_0}\right)^{1/3}\,, \tag{25}$$

$$\mathcal{A}_{+,\times}(f) = \left\{ \lim_{k\to 2\pi f/n_0} \left[\Theta(k-1) H^{(k)}_{+,\times}(e_0) B_k(\bar{\alpha})\right]^{\dagger} \right\}\,, \tag{26}$$

with $\mathcal{M} = m\eta^{3/5}$ the chirp mass of the binary, $n_0 = 2\pi F_{\rm orb}$ the mean frequency at pericenter, e_0 the orbital eccentricity at pericenter, $\Theta(x)$ is the Heaviside step function, and $t^{(o)}_p$ is a time offset that we will discuss in more detail in Sec. V.

In Fig. 2 we show normalized plots of the dispersion modulate plus polarization for the EFB frequency-domain waveforms both under GR and for the same three dispersive cases with the same changing values of D_L corresponding to differing values of $\bar{\alpha}$ as shown in Fig. 1. This illustrative plot shows how the burst is distorted by dispersion effects as the wave propagates and moves away from its source with increasing luminosity distance. The modulated waveforms clearly follow the general envelope of the waveform under GR conditions with the oscillatory behavior being caused by dispersion effects. Again, the variance in waveform response to implementation of dispersive effects is a reflection of the dispersive parameters corresponding to type and strength of the given dispersion effect.

V. MODIFICATIONS TO TIME OF ARRIVAL

Under the EFB framework, the GW signal is modeled as one distinct burst over a finite time interval. To correctly model the full orbital inspiral with multiple GW bursts, it is necessary to implement a timing model over which the EFB waveform evolves accounting for changes in eccentricity, semilatus rectum, and time of the GW signal arrival. Thus we must redefine the EFB waveform equation in Eq. (24) to account for such changes [28], specifically

$$\tilde{h}_{+,\times}(f; M, \eta, p_i, e_i) = \tilde{h}_0 \mathcal{A}_{+,\times}(f; M, \eta, p_i, e_i) \times e^{2\pi i f t^{(o)}_{p,i}(M,\eta,p_i,e_i,t^{(o)}_{p,i-1})}, \tag{27}$$

where we have promoted the previously constant time shift $t^{(o)}_p$ to a function of the binary's parameters. Here, i denotes the values of eccentricity e, semilatus rectum p, and time at which the signal is observed $t^{(o)}_p$ at the end of the $i^{\rm th}$-orbit which are related to the values of these quantities during the previous $i-1$ orbit by the following equations [29–31]:

$$p_i = p_{i-1}\left[1 - \frac{128\pi}{5}\eta\left(\frac{m}{p_{i-1}}\right)^{5/2}\left(1 + \frac{7}{8}e^2_{i-1}\right)\right], \tag{28}$$

$$e_i = e_{i-1}\left[1 - \frac{608\pi}{15}\eta\left(\frac{m}{p_{i-1}}\right)^{5/2}\left(1 + \frac{121}{304}e^2_{i-1}\right)\right], \tag{29}$$

$$t^{(e)}_{p,i} = t^{(e)}_{p,i-1} + \frac{2\pi}{m^{1/2}}\left[\frac{p_{i-1} + \eta m\left(\frac{m}{p_{i-1}}\right)^{3/2} A(\epsilon_i)}{\epsilon_{i-1} + \eta\left(\frac{m}{p_{i-1}}\right)^{5/2} B(\epsilon_i)}\right], \tag{30}$$

where $\epsilon \equiv 1 - e^2$. Arredondo and Loutrel [29] propose the following definitions for the functions A and B,

$$A(\epsilon_i) = a_0 + a_1\epsilon_i\,, \tag{31}$$

$$B(\epsilon_i) = b_0 + b_1\epsilon_i + b_2\epsilon^2_i\,. \tag{32}$$

The a and b coefficients have been calibrated against numerical evolution of the relative Newtonian order osculating equations to obtain [29]:

$$a_0 = a_{0,1} + a_{0,2}\left(\frac{\eta}{1/4}\right)^{a_{0,3}}\left(\frac{p}{10m}\right)^{a_{0,4}}\,, \tag{33}$$

$$a_1 = -16.823395797589278\,, \tag{34}$$

$$b_0 = 170\pi/3 = 178.0235837034216\,, \tag{35}$$

$$b_1 = -139.3766232947201\,, \tag{36}$$

$$b_2 = -1.088578314814299\,, \tag{37}$$

where

$$a_{0,1} = 14.1774066465967\,, \tag{38}$$

$$a_{0,2} = -0.236903393660227\,, \tag{39}$$

$$a_{0,3} = 0.962439591179757\,, \tag{40}$$

$$a_{0,4} = -2.415912280582671\,. \tag{41}$$

The above timing model given by Eqs. (28)-(41) models the evolution of the binary under relative Newtonian order radiation reaction (2.5PN quadrupole radiation). We implement these equations to adjust the time of pericenter t_p and its time shift behavior to reflect the changing values of eccentricity and semilatus rectum due to the loss of orbital energy and angular momentum from GW emission.

When considering dispersion effects, the shift in pericenter passage time in Eq. (30) corresponds to a observer's clock at the location of the binary and does not account for any dispersion effects. Thus we define the

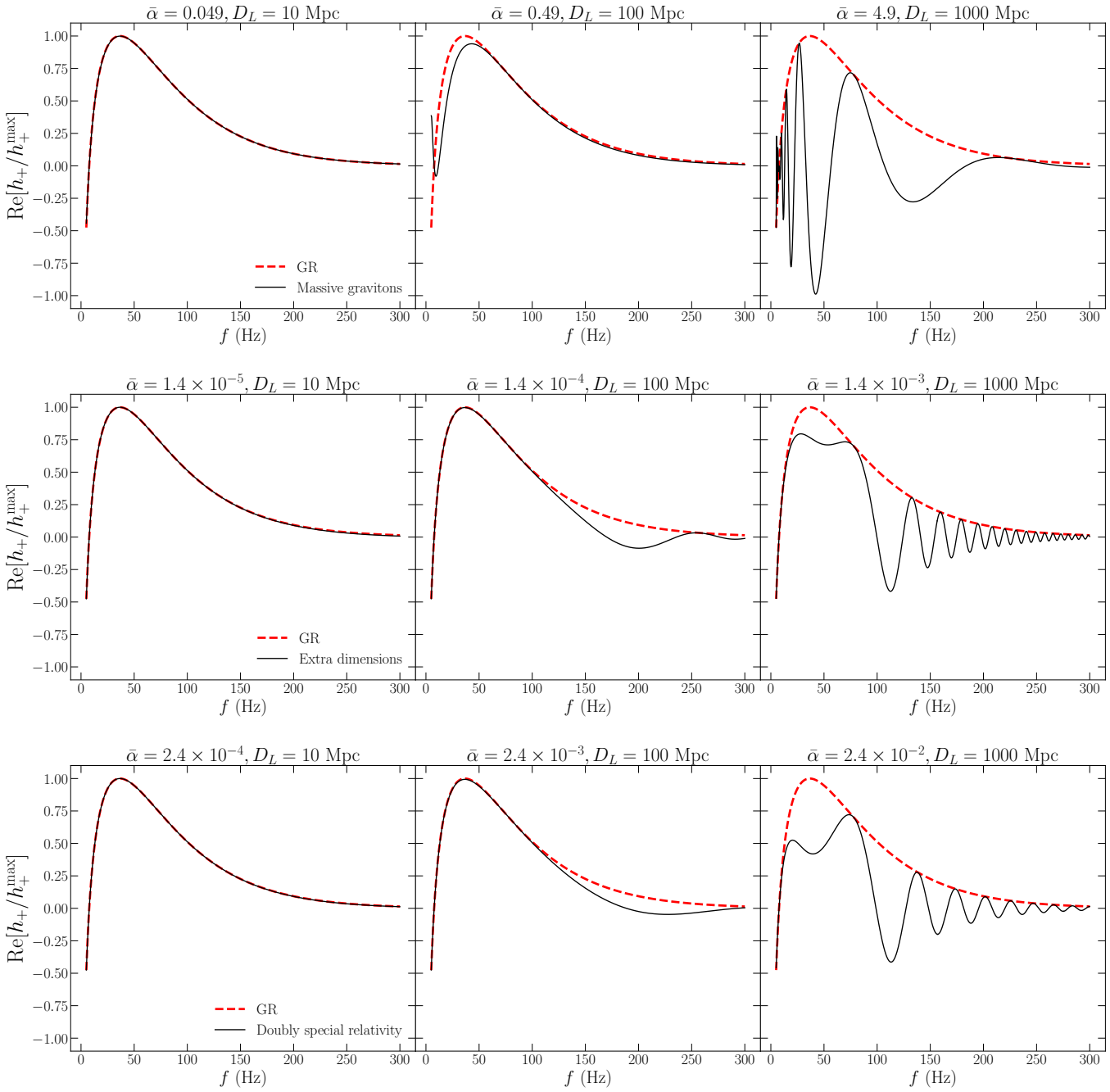

FIG. 2. Comparisons of normalized plus component polarizations in the frequency domain under GR and using the EFB framework for three different dispersive cases: massive gravitons (uppermost panel), extra dimensions (middle panel), and doubly special relativity (bottommost panel). The dashed, red line represents the GR waveform while the black solid lines show the different dispersive waveforms for different values of $\bar{\alpha}$ which assume different values as D_L — which we set at 10 Mpc, 100 Mpc, and 1000 Mpc — increases as denoted by the plot titles. The waveforms are computed using the following parameters: $e = 0.9$, $m = 20M_\odot$, $p = 20m$, $\eta = 0.25$

time variables as $t_p^{(e)}$ because this models the time as an absolute measurement from the moment the burst is emitted. To introduce dispersion effects and obtain a timing model for $t_p^{(o)}$, we must again use the time shift in Eq. (3) to relate $t_p^{(e)}$ in Eq. (30) to the observed time $t_p^{(o)}$ in Eq. (27). To do this, we treat the bursts as discrete objects in time-frequency space with centroids $(f_{\max,i}, t_{p,i}^{(o)})$. Thus, for dispersion caused by massive gravitons, the

shift in the observed pericenter time of the burst is

$$t_{p,i}^{(o)} = t_{p,i-1}^{(o)} + \Delta t_p^{(e)} + \frac{D_L}{2\lambda_g^2}\left[\frac{1}{33 f_{\mathrm{max},i}^2} - \frac{1}{f_{\mathrm{max},i-1}^2}\right], \tag{42}$$

where $\Delta t_p^{(e)} = t_{p,i}^{(e)} - t_{p,i-1}^{(e)}$.

We may make a simplification to Eq. (42), specifically the dispersive term

$$g = \frac{1}{f_{\mathrm{max,i}}^2} - \frac{1}{f_{\mathrm{max,i-1}}^2}, \tag{43}$$

which we have defined as g for simplicity in further references. This dispersive term g can be expanded in terms of k_{max} in Eq. (15), since $f_{\mathrm{max}} = k_{\mathrm{max}} F_{\mathrm{orb}}$. The k_{max} term is a function of e_i which is in turn a function of e_{i-1} through Eq. (29). Likewise, $F_{\mathrm{orb},i}$ is a function of (p_i, e_i), which also map to the previous values through the timing model. It is possible to perform a post-Newtonian (PN) expansion on the dispersive term by series expanding the p_{i-1} term in Eq. (29) about $(m/p_{i-1}) \ll 1$. Then, g becomes a function of e_{i-1} and p_{i-1} without e_i and p_i dependence. We choose to PN expand the dispersive term because it simplifies the g term as previously mentioned now solely depends on $i-1$ terms, which will make waveform parameter estimations simpler and calculations more efficient. Performing the PN expansion to the first order yields the following expression for g_{PN}:

$$\begin{aligned} g_{\mathrm{PN}} = \frac{4}{15}\frac{\eta\pi^3 m^2}{(1+e_{i-1})^{1+2\kappa}}\sqrt{\frac{p_{i-1}}{m}}\big[&-288 \\ &+ 16 e_{i-1}\big(19\kappa - 18\big) - 252 e_{i-1}^2 \\ &+ e_{i-1}^3\big(121\kappa - 252\big)\big], \end{aligned} \tag{44}$$

where $\kappa = 1.1954$.

Fig. 3 shows a two-panel plot highlighting the behavior of g_{PN} in comparison to that of the exact g term for three different binary systems. Table I shows the exact parameters used to compute the values of g and g_{PN}. We see that for each binary type, the PN expanded term closely follows the exact dispersive term with the relative error always staying below 25% and averaging at less than 0.1% for all three binary types. Considering the good similarity between the exact dispersive term and the PN expanded term, we proceed using the PN expansion.

System	$m1[M_\odot]$	$m2[M_\odot]$	$e(0)$	$a(0)$
NS-NS	1.4	1.4	0.9	1360
NS-BH	1.4	10	0.9	535
BH-BH	10	10	0.9	368

TABLE I. Initial parameters used to compute g and g_{PN} for the aforementioned binary systems.

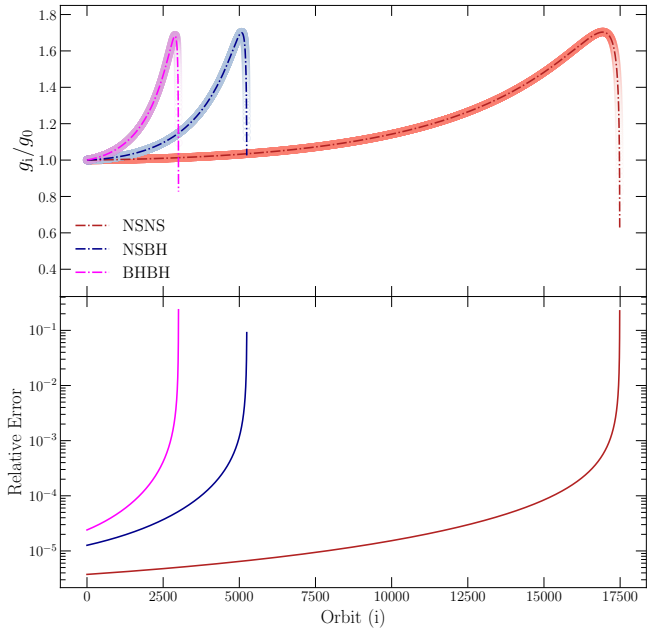

FIG. 3. Upper panel: Comparison between exact EFB timing model dispersive term g (solid dashed lines) and the PN expanded terms g_{PN} (wider, lighter-colored lines) for three different binaries; binary neutron star (red), mixed neutron star/black hole (blue), binary black hole (magenta). The plots span from the 0^{th} orbit with initial conditions in Table I up to the last stable orbit such that $p_i \geq 2m(3+e_i)$. Lower panel: Plot of the relative error in the PN expanded term.

VI. NEXT STEPS

As we continue to study the utility of these newly derived waveforms for dispersive, highly eccentric binary systems, we must also consider how they aid in constraining theories of GR and evaluating the validity of both GR and specific modifications to GR. The next steps in pursuing this understanding would be to perform parameter estimations for different dispersion types and utilizing Fisher analysis to constrain these parameters.

It would also be useful to revisit the discussion of the timing model in Sec. V to generalize the formalism to the broader spectrum of dispersion effects and not just limit our discussion to the massive gravitons case.

We also hope to evaluate data expectations from these waveforms including studying signal-to-noise ratios for different dispersion cases under varying parameters.

ACKNOWLEDGMENTS

A.B. is supported by NSF grant PHY-2348913 and NSF grant PHY-1950830. N.L. is supported by ERC Starting Grant No. 945155–GWmining, Cariplo Foundation Grant No. 2021-0555, MUR PRIN Grant No. 2022-Z9X4XS, and the ICSC National Research Centre funded by NextGenerationEU.

We would also like to thank the University of Florida's IREU program for making this research possible and specifically thank UF professors Paul Fulda and Peter Wass for their commitment to undergraduate research. We also thank the other members of the 2024 IREU cohort and the Gerosa group for their contributions to the program and research experience abroad.

Appendix A: Revisiting Frequency-Domain Effective Fly-By Waveforms

The effective fly-by (EFB) approach seeks to accurately model the GW burst emission from highly eccentric binaries. While a time-domain approach showed strong agreement with numerical leading PN order waveforms [30], frequency-domain waveforms have stumbled on numerical computation issues [30], complicated analytical computations [32], and limitations of suitable approximations [33]. We here revisit the original, leading PN order, frequency-domain EFB waveform from [30], and provide a significant simplification for the construction of current and future EFB waveform templates.

At leading PN order, the two-body dynamics reduce to Keplerian orbits perturbed by 2.5PN order radiation reaction, which constitues the quadrupole approximation of Peters & Mathews [34, 35]. Under the assumption of adiabatic evolution of the orbital elements, the eccentricity e, semilatus rectum p, and mean anomaly ℓ evolve according to [30]:

$$e(t) = e_0 - \frac{304}{15}\eta e_0 \left(\frac{m}{p_0}\right)^{5/2}\left(1+\frac{121}{304}e_0^2\right)\ell(t)\,, \quad \text{(A1)}$$

$$p(t) = p_0\left[1-\frac{64}{5}\eta\left(\frac{m}{p_0}\right)^{5/2}\left(1+\frac{7}{8}e_0^2\right)\ell(t)\right]\,, \quad \text{(A2)}$$

$$\ell(t) = \frac{n_0}{2\pi F_{\rm rr}}\left\{\exp\left[2\pi F_{\rm rr}\left(t-t_p\right)\right]-1\right\}\,, \quad \text{(A3)}$$

where $[e_0, p_0]$ are the values at pericenter, and

$$n_0 = \frac{1}{m^{1/2}}\left(\frac{1-e_0^2}{p_0}\right)^{3/2}\,, \quad \text{(A4)}$$

$$F_{\rm rr} = \frac{96}{10\pi}\frac{\eta}{m}\left(\frac{m}{p_0}\right)^4\left(1+\frac{73}{24}e_0^2+\frac{37}{96}e_0^4\right)\,. \quad \text{(A5)}$$

The quadrupole order waveform polarizations are then given by Eqs. (7), and, when combined with Eqs. (A1)-(A3), are valid for $\ell \in [-\pi, \pi]$. To obtain the time-domain EFB-T waveforms, one applies a resummation procedure originally developed in [36, 37] directly to these waveform polarizations.

However, [30] showed that the Fourier transform of the time-domain waveforms can be obtained analytically by application of the stationary phase approximation (SPA), before performing the resummation procedure. After transforming the waveforms into the form of Eq. (24) and defining $\epsilon = 1-e^2$, application of the SPA gives [30]:

$$\tilde{h}_{+,\times}(f) = -\frac{m^2\eta}{D_L F_{\rm rr}}\sum_{k=1}^{\infty}\left(\frac{\epsilon^\star_{k,-}}{p^\star_{k,-}}\right)\frac{\left[H^{(k)}_{+,\times}(e^\star_{k,-})\right]^\dagger}{\sqrt{2\pi\chi}}e^{i\Psi_\star(k,f)}, \quad \text{(A6)}$$

where $\chi = f/F_{\rm rr}$, $\chi_{\rm orb} = n_0/2\pi F_{\rm rr}$, $\Psi_\star$ is the waveform's stationary phase

$$\Psi_\star(k,f) = k\chi_{\rm orb} - \chi\left[1+\ln\left(\frac{k\chi_{\rm orb}}{\chi}\right)\right] - \frac{\pi}{4} + 2\pi f t_p\,, \quad \text{(A7)}$$

and $[e^\star_{k,-}, p^\star_{k,-}, \epsilon^\star_{k,-}]$ correspond to the time evolving orbital elements evaluated at the stationary point

$$t^\star_{k,-} = t_p + \frac{1}{2\pi F_{\rm rr}}\ln\left(\frac{2\pi f}{k n_0}\right)\,. \quad \text{(A8)}$$

With application of the resummation procedure from [36, 37], the above waveform can be resummed to obtain the EFB-F waveform which has known complications when one attempts to numerically evaluate the model [30], and analytic simplifications to speed up the waveform evaluation are complicated [32].

Instead, we apply a slightly different resummation procedure here. After converting the sum in Eq. (A6) to an integral over k, the integral takes the standard form of a generalized Fourier integral and we apply the SPA again to the stationary phase $\Psi_\star(k,f)$. The new stationary point is given by $k_\star = \chi/\chi_{\rm orb} = 2\pi f/n_0$, and the EFB waveform reduces to

$$\tilde{h}_{+,\times}(f) = -\frac{2\pi}{D_L}\left(\frac{\mathcal{M}^5}{n_0}\right)^{1/3}\mathcal{H}_{+,\times}(f;e_0)e^{2\pi i f t_p}\,, \quad \text{(A9)}$$

where $\mathcal{M} = m\eta^{3/5}$ is the chirp mass, and the Fourier amplitude is given by

$$\mathcal{H}_{+,\times}(f;e_0) = \lim_{k\to 2\pi f/n_0}\left[\Theta(k-1)H^{(k)}_{+,\times}(e^\star_{k,-})\right]^\dagger\,, \quad \text{(A10)}$$

with $\Theta(x)$ the Heaviside step function, which accounts for the fact that the original sum over k begins at $k=1$. It is worth noting that, after both applications of the SPA (first over time, then over k for resummation),

$$\lim_{k\to 2\pi f/n_0}[e^\star_{k,-}, p^\star_{k,-}, \epsilon^\star_{k,-}] = [e_0, p_0, \epsilon_0], \quad \text{(A11)}$$

and thus,

$$\mathcal{H}_{+,\times}(f;e_0) = \lim_{k\to 2\pi f/n_0}\left[\Theta(k-1)H^{(k)}_{+,\times}(e_0)\right]^\dagger\,, \quad \text{(A12)}$$

which is simply the time-domain harmonic coefficient evaluated at continuous frequency f instead of the discrete harmonic index k. This should not be surprising since adiabatic radiation reaction, by it's nature, should have little effect on the dynamics of the binary over a single orbit.

[1] N. Loutrel, N. Yunes, and F. Pretorius, Phys. Rev. D **90**, 104010 (2014), arXiv:1404.0092 [gr-qc].
[2] N. Yunes, K. Yagi, and F. Pretorius, Phys. Rev. D **94**, 084002 (2016), arXiv:1603.08955 [gr-qc].
[3] Z. Carson and K. Yagi, (2020), 10.1007/978-981-15-4702-$7_41 - 1$, arXiv:2011.02938 [gr-qc].
[4] S. Mirshekari, N. Yunes, and C. M. Will, Phys. Rev. D **85**, 024041 (2012), arXiv:1110.2720 [gr-qc].
[5] C. M. Will, Phys. Rev. D **57**, 2061 (1998), arXiv:gr-qc/9709011.
[6] V. A. Rubakov and P. G. Tinyakov, Phys. Usp. **51**, 759 (2008), arXiv:0802.4379 [hep-th].
[7] K. Hinterbichler, Rev. Mod. Phys. **84**, 671 (2012), arXiv:1105.3735 [hep-th].
[8] C. de Rham, Living Rev. Rel. **17**, 7 (2014), arXiv:1401.4173 [hep-th].
[9] A. S. Sefiedgar, K. Nozari, and H. R. Sepangi, Phys. Lett. B **696**, 119 (2011), arXiv:1012.1406 [gr-qc].
[10] G. Amelino-Camelia, Phys. Lett. B **510**, 255 (2001), arXiv:hep-th/0012238.
[11] J. Magueijo and L. Smolin, Phys. Rev. Lett. **88**, 190403 (2002), arXiv:hep-th/0112090.
[12] G. Amelino-Camelia, Nature **418**, 34 (2002), arXiv:gr-qc/0207049.
[13] P. Horava, JHEP **03**, 020 (2009), arXiv:0812.4287 [hep-th].
[14] P. Horava, Phys. Rev. D **79**, 084008 (2009), arXiv:0901.3775 [hep-th].
[15] S. I. Vacaru, Gen. Rel. Grav. **44**, 1015 (2012), arXiv:1010.5457 [math-ph].
[16] D. Blas and H. Sanctuary, Phys. Rev. D **84**, 064004 (2011), arXiv:1105.5149 [gr-qc].
[17] G. Calcagni, Phys. Rev. Lett. **104**, 251301 (2010), arXiv:0912.3142 [hep-th].
[18] G. Calcagni, Adv. Theor. Math. Phys. **16**, 549 (2012), arXiv:1106.5787 [hep-th].
[19] G. Calcagni, JHEP **01**, 065 (2012), arXiv:1107.5041 [hep-th].
[20] G. Calcagni, Eur. Phys. J. C **77**, 291 (2017), arXiv:1603.03046 [gr-qc].
[21] V. A. Kostelecký and M. Mewes, Phys. Lett. B **757**, 510 (2016), arXiv:1602.04782 [gr-qc].
[22] H. Wahlquist, General Relativity and Gravitation **19**, 1101 (1987).
[23] K. Martel and E. Poisson, Phys. Rev. D **60**, 124008 (1999), arXiv:gr-qc/9907006 [gr-qc].
[24] C. Moreno-Garrido, E. Mediavilla, and J. Buitrago, **274**, 115 (1995).
[25] B. Moore, T. Robson, N. Loutrel, and N. Yunes, Class. Quant. Grav. **35**, 235006 (2018), arXiv:1807.07163 [gr-qc].
[26] L. Wen, Astrophys. J. **598**, 419 (2003), arXiv:astro-ph/0211492.
[27] M. Turner, Astrophys. J. **216**, 610 (1977).
[28] N. Loutrel, T. Tanaka, and N. Yunes, Phys. Rev. D **98**, 064020 (2018), arXiv:1806.07431 [gr-qc].
[29] J. N. Arredondo and N. Loutrel, Classical and Quantum Gravity **38**, 165001 (2021), arXiv:2101.10963 [gr-qc].
[30] N. Loutrel, Classical and Quantum Gravity **37**, 075008 (2020), arXiv:1909.02143 [gr-qc].
[31] N. Loutrel and N. Yunes, Classical and Quantum Gravity **34**, 135011 (2017), arXiv:1702.01818 [gr-qc].
[32] N. Loutrel, Class. Quant. Grav. **38**, 015005 (2021), arXiv:2003.13673 [gr-qc].
[33] N. Loutrel, Class. Quant. Grav. **40**, 215004 (2023), arXiv:2304.00836 [gr-qc].
[34] P. C. Peters and J. Mathews, Phys. Rev. **131**, 435 (1963).
[35] P. C. Peters, Phys. Rev. **136**, B1224 (1964).
[36] N. Loutrel and N. Yunes, Class. Quant. Grav. **34**, 044003 (2017), arXiv:1607.05409 [gr-qc].
[37] E. Forseth, C. R. Evans, and S. Hopper, Phys. Rev. D **93**, 064058 (2016), arXiv:1512.03051 [gr-qc].